Stochastic multiscale model for carbonate rocks

B. Biswal,[1,2] P.-E. Øren,[3] R. J. Held,[4] S. Bakke,[3] and R. Hilfer[1,5]
[1]*ICP, Universität Stuttgart, Pfaffenwaldring 27, 70569 Stuttgart, Germany*
[2]*S. V. College, University of Delhi, New Delhi-110 021, India*
[3]*Numerical Rocks AS, N-7041 Trondheim, Norway*
[4]*Statoil ASA, N-7005 Trondheim, Norway*
[5]*Institut für Physik, Universität Mainz, 55099 Mainz, Germany*
(Received 9 January 2007; published 12 June 2007)

A multiscale model for the diagenesis of carbonate rocks is proposed. It captures important pore scale characteristics of carbonate rocks: wide range of length scales in the pore diameters; large variability in the permeability; and strong dependence of the geometrical and transport parameters on the resolution. A pore scale microstructure of an oolithic dolostone with generic diagenetic features is successfully generated. The continuum representation of a reconstructed cubic sample of sidelength 2 mm contains roughly 42×10^6 crystallites and pore diameters varying over many decades. Petrophysical parameters are computed on discretized samples of sizes up to 1000^3. The model can be easily adapted to represent the multiscale microstructure of a wide variety of carbonate rocks.

DOI: 10.1103/PhysRevE.75.061303 PACS number(s): 81.05.Rm, 02.70.−c, 47.56.+r, 91.60.Np

A complex multiscale problem of considerable practical importance is the physics of carbonate rocks that contain nearly half of the world's current hydrocarbon reserves. Model reconstruction of the three-dimensional (3D) pore scale microstructure of carbonates is crucial for understanding the physics of flow processes [1,2]. Although a number of pore scale models and 3D reconstruction methods are available for sandstones [2–5], developing a similar model for carbonates [6,7] has been difficult.

In carbonate rocks, contrary to sandstones [8], permeability can vary by 2 to 3 decades at fixed porosity [9,10]. Pore diameters range over many decades in length scales and the carbonate textures show a strongly correlated disorder [11]. Geometrical and petrophysical parameters of carbonates depend strongly on the resolution. Calcite-dolomite crystallites may vary in size from 10^{-7} to 10^{-3} m. A reasonable discretization requires a voxel size of at least 10^{-8} m to resolve the smallest of the crystallites. For a cubic sample of length 10^{-2} m, the discretized pore space representation requires roughly 10^{18} digits, i.e., nearly 10^6 terabytes of storage space. Thus traditional discretization fails, and a novel modeling approach is needed to represent the microstructure of carbonates.

We propose a stochastic geometrical model for the diagenetic processes in carbonate rocks. It reproduces both the complex pore scale geometry and the basic petrophysical properties. It is a continuum model that represents the pore scale microstructure at arbitrary resolution. The carbonate rock is viewed as a random but correlated sequence of points decorated with crystallites. The model is defined as follows.

a. Continuum representation. Consider a sample occupying a bounded region $\mathbb{S}\subset\mathbb{R}^3$. The state space of the continuum model with N crystallites is the set

$$\Omega_N = (\mathbb{S}\times[R_{\min},R_{\max}]\times\mathbb{E}\times\{1,2,\ldots,g\})^N \tag{1}$$

of all sequences $\omega=(\omega_0,\omega_1,\ldots,\omega_N)\in\Omega_N$ of length N where $\mathbb{E}=\{\mathbf{x}\in\mathbb{R}^3:|\mathbf{x}|=1\}$ is the unit sphere, and $[R_{\min},R_{\max}]\subset\mathbb{R}^1$. An element

$$\omega_i = (\mathbf{x}_i,R_i,\mathbf{a}_i,T_i) \tag{2}$$

of the sequence represents a dolomite or carbonate crystallite at spatial position $\mathbf{x}_i\in\mathbb{S}$ with size R_i, orientation $\mathbf{a}_i$, and type T_i. A crystallite is a convex set such as a sphere or polyhedron, etc. Every sequence ω with $\mathbf{x}_i\in\mathbb{S}$ defines a model. The model is further specified by a probability distribution Prob on the space Ω of sequences.

b. Primordial filter function. Assume that a primordial depositional texture is given as a grayscale image G and represented mathematically as a bounded, but not necessarily continuous function $G:\mathbb{S}\to[0,1]$. This input function $G(\mathbf{x})$ is generated from the image analysis of the original sample. It serves to correlate the location and properties of the deposited crystallites with that of the original depositional texture through the functions:

$$R_i=\mathcal{R}(G(\mathbf{x}_i));\quad \mathbf{a}_i=\mathcal{A}(G(\mathbf{x}_i));\quad T_i=\mathcal{T}(G(\mathbf{x}_i)), \tag{3}$$

where $\mathcal{R}:[0,1]\to[R_{\min},R_{\max}]\cup\{0\}$, $\mathcal{A}:[0,1]\to\mathbb{E}$, and $\mathcal{T}:[0,1]\to\{1,2,\ldots,g\}$. These correlations are specified by quantitative image analysis and measurements done on 2D sections of the original sample.

c. Deposition of points. Binomial point processes are used as the basic trial process in which points $\mathbf{x}_i$ with associated radius R_i are chosen randomly with uniform distribution in $\mathbb{S}\subset\mathbb{R}^3$ subject to overlap constraints. More precisely, we set $\mathrm{Prob}(\Omega_c)=0$ for

$$\Omega_c=\{\omega\in\Omega:\exists i,j,o(\omega_i,\omega_j)\notin(0,\lambda_i]\}, \tag{4}$$

where $o(\omega_i,\omega_j)=\frac{R_i+R_j-|\mathbf{x}_i-\mathbf{x}_j|}{R_i+R_j-|R_i-R_j|}$ is the measure of overlap between the grains ω_i and ω_j. The compaction parameter $\lambda_i=\Lambda(G(\mathbf{x}_i))$, with $\Lambda:[0,1]\to[\lambda_{min},\lambda_{max}]$ and $0<\lambda_{min},\lambda_{max}<1$. Matrix connectivity is ensured because $\lambda_i>0$ leads to finite overlap between each deposited grain with an existing one. Porosity and pore space connectivity depends on the density of points deposited in $\mathbb{S}\subset\mathbb{R}^3$ for a given grain size distribution.

d. Vuggy porosity. The probability distribution on the space of sequences vanishes, $\mathrm{Prob}(\Omega_v)=0$, for

$$\Omega_v = \{\omega \in \Omega: \exists\, 0 \leqslant i \leqslant N, \mathcal{R}(G(\mathbf{x}_i)) = 0\}. \tag{5}$$

In vuggy pore regions, $G(\mathbf{x})=0$ and in this way vugginess is controlled by the primordial depositional texture.

e. Grain decoration. At each deposited point $\mathbf{x}_i$, a crystallite is attached by placing a geometric object of type T_i and orientation $\mathbf{a}_i$ according to the depositional texture [Eq. (3)]. Equation (4) only ensures overlap between associated spherical grains. For other types of grains, we define a grain size $d_i(R_i)$ such that the grain overlap and the matrix connectivity is retained. The sample is fully characterized by a list of N quadruples $(\mathbf{x}_i, d_i, \mathbf{a}_i, T_i)$ of deposited points, associated grain sizes, orientations, and types.

The model described above can be used to reconstruct the pore scale microstructure of a wide variety of carbonate rocks. However, the computational implementation of the model depends on the geometry and textures present and, therefore, may vary from sample to sample. In this paper we focus on oolithic dolostones and the feasibility of the microscopic modeling for this type of carbonate rock. We present in detail the reconstruction of one sample that contains vuggy porosity and two distinct crystallite size distributions within ellipsoidal primordial facies (Fig. 1). The inner cores of ooids contain dolomitized crystallites with radii in the range of $1-10$ μm and the thin isopachous layers (around ooids) contain dolomite cement grains with radii in the range of $5-25$ μm. The sample features diagenetic replacive dolomitization, isopachous or intergranular dolomitization, and the presence of dissolution vugs. The matrix space (Fig. 1) shows a large number of smaller grains around bigger grains and the porosity is roughly in the range of 0.25–0.3.

Consider a cubic sample $\mathbb{S}$ of sidelength $\ell=100$ in dimensionless units. The unit of length of the primordial geometry is 20 μm, so ℓ correpsonds to 2 mm. The dimensionless crystallite size intervals in the ooids and isopachous layer are [0.05, 0.5] and [0.25, 1.25], respectively. The model requires millions of grains to specify the pore scale microstructure of this small sample. With each added point, the CPU time needed for checking the overlap rule (4) grows. It is computationally efficient to divide $\mathbb{S}\subset\mathbb{R}^3$ into smaller nonoverlapping cubic cells $\mathbb{U}$ each of sidelength l i.e., $\mathbb{S}=\mathbb{U}_1\cup\mathbb{U}_2\cup\mathbb{U}_3\cdots\cup\mathbb{U}_m$, where $m=(\ell/l)^3$.

Points are added to each cell satisfying the overlap rule (4) for all the existing points in the cell and the neighboring cells. For the jth deposited point in each cell $\mathbb{U}$,

$$R_j = R_{min} + \left[1 - \frac{j}{n}\right]\xi\Delta R, \tag{6}$$

where $\Delta R=R_{max}-R_{min}$ and ξ is a uniform random number in (0, 1). This ensures a uniform but random distribution of R_i in $[R_{min}, R'_{max}]$ with R'_{max} decreasing with each deposit. This achieves the hierarchical filling of space by many smaller grains around bigger grains as in the original sample. In each cell $n=\rho l^3/(\frac{4}{3}\pi R^3_{max})$ number of points are deposited. The point density ρ is adjusted so that the porosity of the grain decorated realization matches the target porosity. This is measured by discretizing many such trial realizations at high resolution (see below). Simultaneously, the pore space connectivity is verified using the Hoshen-Kopelman algorithm [12].

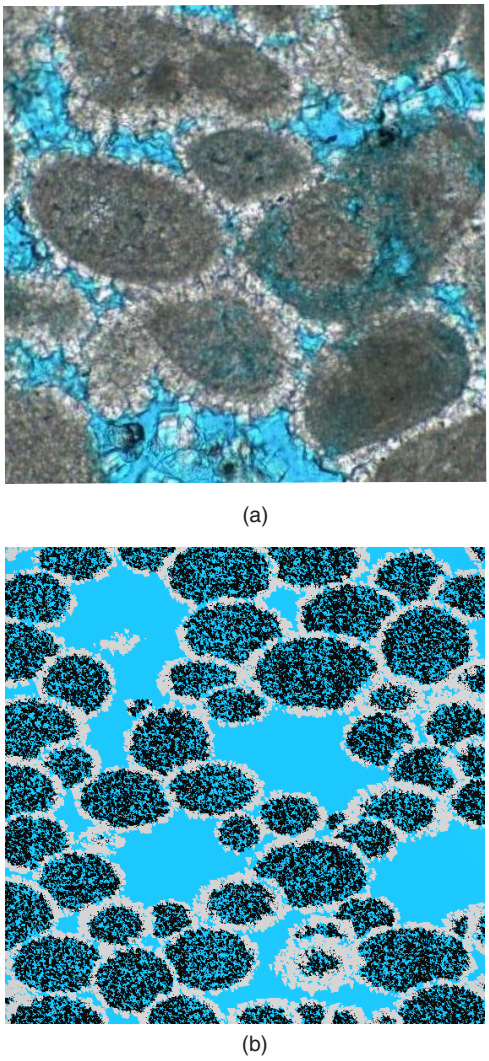

(a)

(b)

FIG. 1. (Color online) Top: 2D section of original oolithic dolostone ($\ell=0.6$ mm). Bottom: Reconstructed sample ($\ell=2$ mm).

The primordial filter function $G(\mathbf{x})$ is constructed from a sedimentation of polydisperse oblate elliptical ooids in $\mathbb{S}\subset\mathbb{R}^3$ [13]. A small fraction of these were removed to generate vuggy pores and the remaining ellipsoids were enlarged by 20% of their size to reduce the interellipsoid pore space. The kth oblate spheroid represented by $\{\mathbf{r}_k, s_k, e_k\}$ is centered at $\mathbf{r}_k=(x_k, y_k, z_k)$ with semiaxes lengths $a_k=e_k s_k$, $b_k=e_k s_k$, and $c_k=s_k$. The grayscale primordial filter function is defined as

$$G(\mathbf{x}) = \begin{cases} 1-(d_k/s_k) & \text{if any } d_k < s_k \\ 0 & \text{otherwise,} \end{cases} \tag{7}$$

where $d_k=[(x_1-x_k)^2/e_k^2+(x_2-y_k)^2/e_k^2+(x_3-z_k)^2]^{1/2}$.

We first deposit N_1 points corresponding to the isopachous layers by choosing $l=5$, $\lambda_i=\Lambda(G(\mathbf{x}_i))=0.6$, $\rho=40$,

$R_{min}=0.25$, and $R_{max}=1.25$. Points $\mathbf{x}_i$ are added to $\mathbb{S}$ with $\text{Prob}(\Omega_1)=0$, for

$$\Omega_1=\{\omega\in\Omega:\exists\, 0\leqslant i\leqslant N, G(\mathbf{x}_i)\notin(0,0.125)\}. \quad (8)$$

The isopachous layers contain dolomite crystallites. First these N_1 points are decorated with equilateral rhombohedra. Each rhombohedron $\mathbb{G}_i$ (before rotation) centered at $\mathbf{x}_i$ is the intersection of three pairs of parallel planes each separated by a distance d_i and tilted by an angle $\alpha=-15°$ about the three coordinate axes, respectively. The equations of these six planes are

$$\mathbf{n}_j\cdot\mathbf{x}\pm\frac{d_i}{2}=0,\quad j=1,2,3, \quad (9)$$

where $\mathbf{n}_1=(\cos\alpha,0,-\sin\alpha)$, $\mathbf{n}_2=(-\sin\alpha,\cos\alpha,0)$, $\mathbf{n}_3=(0,-\sin\alpha,\cos\alpha)$, and d_i is chosen such that the volume of $\mathbb{G}_i$ equals the volume of the associated excluded volume sphere. Sufficiently large overlap guarantees matrix connectivity. The orientation $\mathbf{a}_i$ of a crystallite $\mathbb{G}_i$ is represented by the unit quaternion

$$\mathbf{q}_i=\mathcal{A}(G(\mathbf{x}_i))=\mathcal{Q}_{i3}\mathcal{Q}_{i2}\mathcal{Q}_{i1}, \quad (10)$$

where the unit quaternion $\mathcal{Q}_{ij}$ represents a rotation of θ_j about the vector $\mathbf{e}_j$. So, $\mathbf{q}_i$ defines a sequence of three rotations of θ_1, θ_2, and θ_3 about the coordinate axes $\mathbf{e}_1=(1,0,0)$, $\mathbf{e}_2=(0,1,0)$, and $\mathbf{e}_3=(0,0,1)$, respectively. For each $\mathbb{G}_i$, the origin is fixed at $\mathbf{x}_i$ and $\theta_j=-20\eta$ deg, where η is a uniform random number in [0,1].

Points corresponding to the ooids fillings are then added by choosing $l=1.5$, $\lambda_i=\Lambda(G(\mathbf{x}_i))=0.65$, $\rho=40$, $R_{min}=0.05$, and $R_{max}=0.5$. Points at $\mathbf{x}_i$ are added to $\mathbb{S}$ with $\text{Prob}(\Omega_2)=0$, for

$$\Omega_2=\{\omega\in\Omega:\exists\, 0\leqslant i\leqslant N,\ G(\mathbf{x}_i)<0.1\} \quad (11)$$

and only if $\mathbf{x}_i\notin\mathbb{M}_1$ where $\mathbb{M}_1=\mathbb{G}_1\cup\mathbb{G}_2\cdots\cup\mathbb{G}_{N_1}$. These N_2 points are also decorated with rhombohedra and added to the list. To check if $\mathbf{x}_i\notin\mathbb{M}_1$, or in general, to check if a point $\mathbf{p}\in\mathbb{G}_i$, we first translate the coordinate axes to the center of the grain $\mathbb{G}_i$, followed by an inverse rotation given by $\mathbf{q}_i^{-1}$,

$$\mathbf{p}'=\mathbf{p}-\mathbf{x}_i;\quad \mathbf{p}'_r=\mathbf{q}_i^{-1}\mathbf{p}'(\mathbf{q}_i^{-1})^*, \quad (12)$$

where $(\cdot)^*$ is quaternion conjugation. The point $\mathbf{p}\in\mathbb{G}_i$ if

$$\left(\mathbf{n}_j\cdot\mathbf{p}'_r+\frac{d_i}{2}\right)\left(\mathbf{n}_j\cdot\mathbf{p}'_r-\frac{d_i}{2}\right)<0,\quad j=1,2,3. \quad (13)$$

$G(\mathbf{x})=0$ holds in the interellipsoid regions and in the vuggy pores. The matrix space $\mathbb{M}$ consists of the $N=N_1+N_2\sim4.1\times10^7$ deposited rhombohedral crystallites. One face of the reconstructed three-dimensional oolithic dolostone is shown in Fig. 1.

The above model is defined in the continuum and can be discretized at arbitrary resolutions. The cubic sample is subdivided into a grid of cubic voxels of sidelength a. The sidelength of the sample is $M=\ell/a$ voxels. In our discretization, a voxel located at position $\mathbf{p}=(p_1a,p_2a,p_3a)$ is chosen as matrix if all of the following nine points fall within a grain $\mathbb{G}_i$, $i=1,2,\ldots,N$.

$$\mathbf{p}_j=\mathbf{p}+\frac{a}{2}(\mathbf{e}_1+\mathbf{e}_2+\mathbf{e}_3)+\frac{a}{4}\mathbf{t}_j;\quad j=0,1,\ldots,8, \quad (14)$$

where $\mathbf{t}_0=(0,0,0)$, $\mathbf{t}_1=(1,1,1)$, $\mathbf{t}_2=(-1,-1,-1)$, $\mathbf{t}_3=(1,1,-1)$, $\mathbf{t}_4=(-1,-1,1)$, $\mathbf{t}_5=(1,-1,1)$, $\mathbf{t}_6=(-1,1,-1)$, $\mathbf{t}_7=(-1,1,1)$, and $\mathbf{t}_8=(1,-1,-1)$. If they all fall in pore space, the voxel is resolved as pore, otherwise the voxel status is *undecided* at the current resolution. Although alternate and more accurate discretization methods can be chosen, the above rule is computationally simple and sufficient for the following analysis.

Porosity and petrophysical parameters of carbonates show strong dependence on resolution. Four discretizations of the reconstructed sample are shown in Fig. 2. The fraction of undecided voxels decreases with higher resolution and as a result, porosity increases significantly with higher resolution as seen in real carbonates. The fraction of resolved matrix, pore, and undecided voxels for different resolutions are plotted in Fig. 3. A rough estimate of the porosity for the fully resolved sample is obtained from the extrapolation to $a=0$ and is close to the targeted value 0.25–0.3. The resolved pore scale microstructure exhibits the intergranular and intragranular porosity of the oolithic structure. A systematic analysis of the scale and resolution dependence has been carried out by measuring petrophysical parameters [14] on the digitized samples. The undecided voxels are alternately converted to matrix (solid) and pore (void) voxel for this analysis.

For permeability, the steady state Stokes equation: $\mu\nabla^2\mathbf{v}=\nabla p$, $\nabla\cdot\mathbf{v}=0$ is solved using a lattice Boltzmann method with boundary condition $\mathbf{v}=\mathbf{0}$ on the solid walls. Effective permeability k_x computed by applying a pressure difference of Δp along the x-axes and using Darcy's law is plotted in Fig. 3 as a function of resolutions. The scattered symbols indicate the permeability computed from nonoverlapping subsamples extracted from the full sample and show the large variability within the same sample.

For elastic moduli, the basic equations of elastostatics: $\nabla\cdot\tau=0$, $\tau=\mathbf{C}:\varepsilon$ are solved by a finite element method using an energy representation of the linear elastic equations with periodic boundary conditions on the faces. The magnitude of the shear moduli and its dependence on porosity plotted in Fig. 4 match well with the findings on 3D tomographic models of similar carbonate rocks [7].

For computing the formation factor, electrostatic equations $\nabla\cdot\mathbf{J}=0$, $\mathbf{J}=\sigma^{(\omega)}\nabla\Phi$ are solved numerically by a finite difference method with boundary condition $\nabla\Phi\cdot\mathbf{n}=0$ on the solid walls. The directional conductivities σ_i are computed with the potential gradient applied across the medium and no flow boundary condition laterally. The anisotropy in Fig. 4 is due to the occurrence and orientations of the vugs, primordial ooids, and the crystallites.

The proposed model reproduces the resolution dependent porosity and the permeability scatter of the original oolithic dolostone. It captures many other crucial features of the dolomites: scale dependent intergranular porosity over many

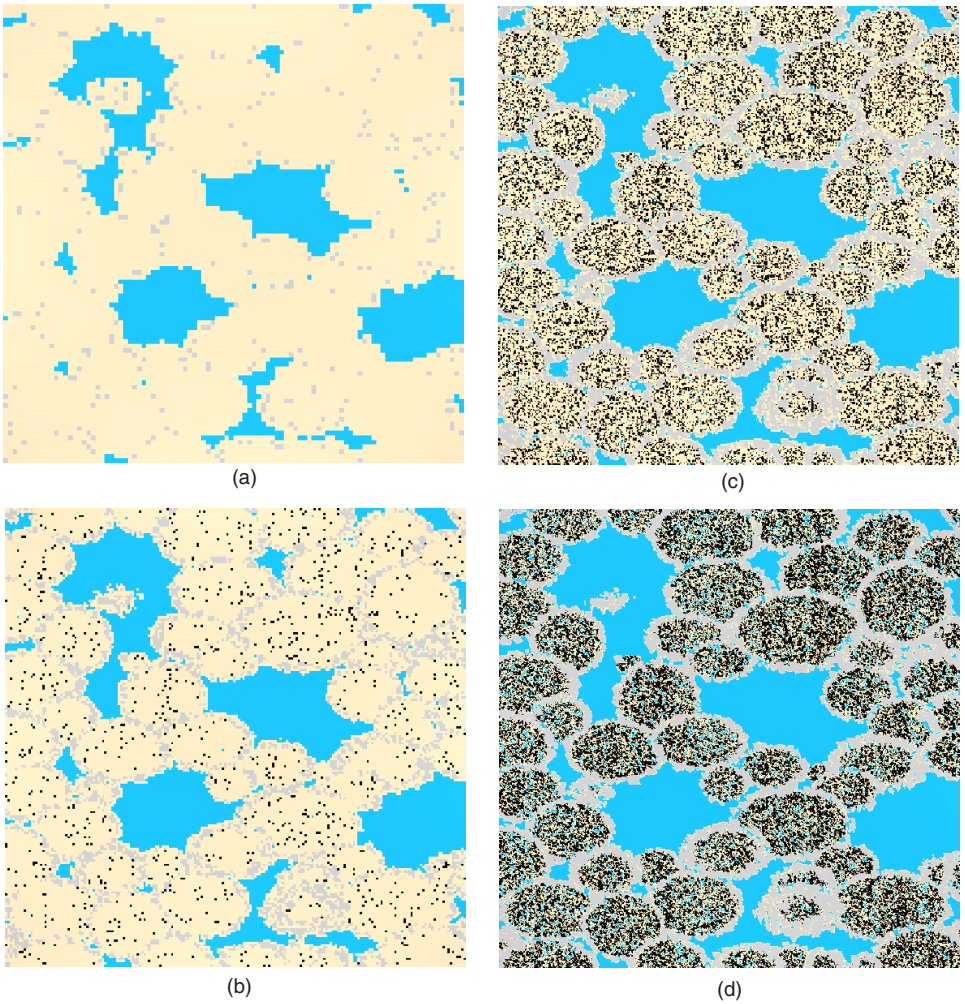

FIG. 2. (Color online) Discretized samples at four resolutions: $a=1\times 20\ \mu$m, $M=\ell/a=100$ (a), $a=0.5\times 20\ \mu$m, $M=\ell/a=200$ (b), $a=0.25\times 20\ \mu$m, $M=\ell/a=400$ (c), and $a=0.125\times 20\ \mu$m, $M=\ell/a=800$ (d). At $a=1\times 20\ \mu$m (a), nearly all voxels are unresolved (light gray) and the discretization significantly differs from the fully resolved ($a=0$) image shown in Fig. 1(b). As the voxel size decreases, more and more of the undecided voxels (light gray) are resolved to pore (dark gray) or matrix (medium gray and black). [Color codes in the online figure: black (intra-ooid grains), gray (grains in the isopachous layer), blue (pore), and peach (undecided voxels).

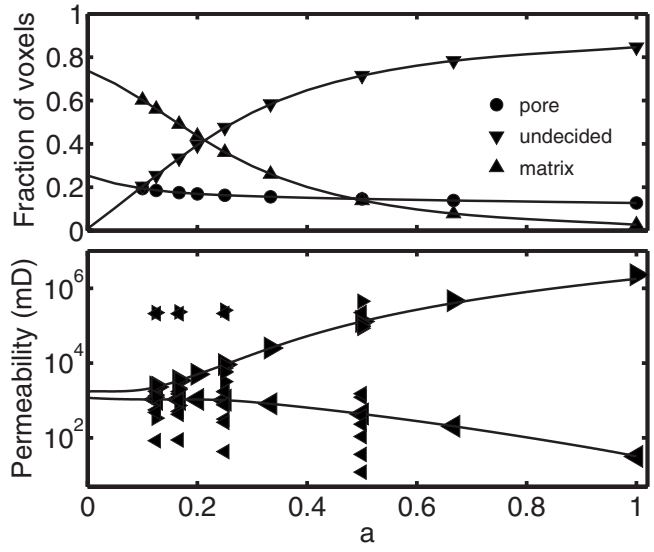

FIG. 3. Top: Fraction of resolved matrix, pore, and undecided voxels at different resolutions. Bottom: Absolute permeability computed on the sample and on subsamples (smaller symbols). Undecided voxels are converted alternately to matrix (◀) or to pore (▶). Solid lines are extrapolations. The abscissa is the resolution a in units of 20 μm.

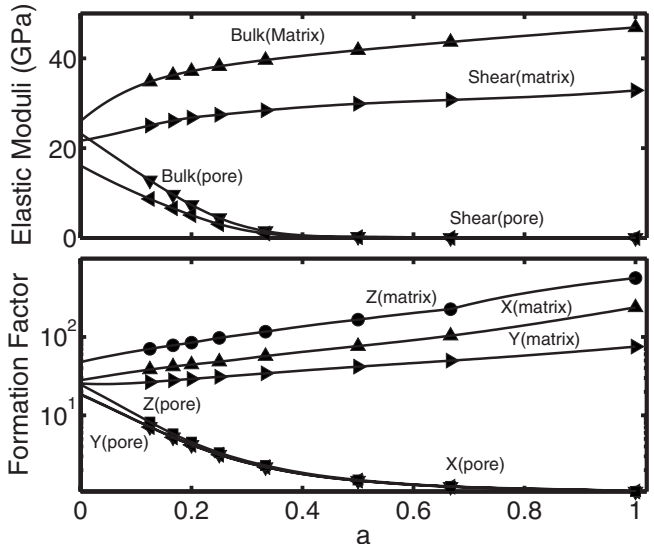

FIG. 4. Top: Bulk moduli and shear moduli computed from the samples at different levels of discretizations. Bottom: Formation factors computed from the same samples in X, Y, and Z directions. Solid lines are extrapolations in both plots. Undecided voxels are alternately converted to a matrix or to a pore. The abscissa is the resolution a in units of 20 μm.

decades, vuggy porosity, a percolating pore space, a fully connected matrix space, strong correlations from primordial depositional textures, and partial dolomitization. The continuum representation provides a practical data structure for representing the complex pore scale microstructure of the carbonates that range over many decades in length scales. Permeabilities vary over three decades within the same sample. For a fixed porosity, transport properties depend upon the primordial geometry, the packing density, and compaction. The model reconstruction of an oolithic dolostone has roughly 42×10^6 crystallites, pore diameters varying in the range of 4 to 5 decades, and petrophysical parameters that can vary greatly. The physical parameters are evaluated from discretized samples of size up to 1000^3 voxels. This resolution can be increased arbitrarily to any desired value. The model can be easily adapted to reconstruct the pore texture of a wide variety of carbonate rocks. Our model thus overcomes major stumbling blocks in the reconstruction of the pore scale microstructure of carbonate rocks.

The authors are grateful to Statoil ASA, Norway for permission to publish early and for financial support.

[1] M. Sahimi, Rev. Mod. Phys. **65**, 1393 (1993).
[2] P. M. Adler, *Porous Media–Geometry and Transports* (Butterworth-Heinemann, Boston, 1992).
[3] A. P. Roberts, Phys. Rev. E **56**, 3203 (1997).
[4] C. L. Y. Yeong and S. Torquato, Phys. Rev. E **57**, 495 (1998).
[5] H. Hamzehpour and M. Sahimi, Phys. Rev. E **74**, 026308 (2006).
[6] H. Okabe and M. J. Blunt, Phys. Rev. E **70**, 066135 (2004).
[7] C. H. Arns, M. A. Knackstedt, and K. R. Mecke, Phys. Rev. Lett. **91**, 215506 (2003).
[8] C. P. Fernandes, F. S. Magnani, P. C. Philippi, and J. F. Däian, Phys. Rev. E **54**, 1734 (1996).
[9] F. S. Anselmetti, S. M. Luthi, and G. P. Eberli, AAPG Bull. **82**, 1815 (1998).
[10] C. H. Moore, *Carbonate Diagenesis and Porosity* (Elsevier, Amsterdam, 1989).
[11] Y.-Q. Song, S. Rye, and P. Sen, Nature (London) **406**, 178 (2000).
[12] D. Stauffer and A. Aharony, *Introduction to Percolation Theory* (Taylor and Francis, London, 1992).
[13] S. Bakke and P. Øren, SPE J. **2**, 136 (1997).
[14] R. Hilfer and C. Manwart, Phys. Rev. E **64**, 021304 (2001).